Phys. Chem. Solids 31, 1381 (1970).
[23]R. N. Ghoshtagore, Phys. Status Solidi 20, K89 (1967).
[24]M. Yoshida and K. Saito, Japan. J. Appl. Phys. 6, 573 (1967).
[25]M. Yoshida and K. Furusho, Japan. J. Appl. Phys. 3, 541 (1964).

PHYSICAL REVIEW B VOLUME 3, NUMBER 8 15 APRIL 1971

Symmetry Analysis of Electroreflectance Spectra

N. Bottka* and J. E. Fischer
Michelson Laboratory, China Lake, California 93555
(Received 22 September 1969; revised manuscript received 28 September 1970)

A systematic study is undertaken of the polarization anisotropies observed in electroreflectance, with the objective of obtaining information about the Brillouin zone (BZ) location and $E(k)$ topology of the transition. The analysis permits the extraction of such symmetry information from properly designed experiments, independent of the details of the spectral line shape, and magnitude and inhomogeneity of the modulating field. It is shown that transitions originating from ⟨111⟩ and ⟨100⟩ directions in the BZ can be identified. Criteria are established for determining the validity of the weak-field approximation in calculations of the electro-optic effect, and for determining the effect of the electric field on the transition matrix element. The effect of the electric field on band degeneracies is considered, and their correlation to observed anisotropies is discussed. Comparison of the analytical results with electroreflectance measurements in germanium is made.

I. INTRODUCTION

Semiempirical band models depend on an accurate correlation of optical spectra to critical points in the band structure, as characterized by transition energy, location in the Brillouin zone (BZ), and topology of the interband energy surface.[1] Only the first of these criteria of identification can be directly read out from static reflectance spectra. Consequently, band-structure analysis faces the problem of unfolding the observed one-dimensional sequence of transition energies into the three dimensions of the BZ.

As the source of experimental information in this assignment procedure, modulated reflectance is superior to static reflectance for two reasons. First, the modulated response correlates to localized rather than extended regions in the BZ,[2] thereby giving experimental information which is more directly comparable with calculated energy gaps. Second, modulation by an electric field or a stress establishes a preferred direction and lowers the symmetry of the sample crystal; consequently, anisotropies of the reflectance response are observed as the modulating vector rotates relative to the crystal frame.[3–6] Of the two, the latter has received the least attention. It is the object of this work to examine the diagnostic potential of these anisotropies in electroreflectance (ER).

In an attempt to explain these anisotropies, Phillips[7] suggested that they occur at two different levels. *Nontensorial* anisotropies arise from the intraband mixing caused by the electric field (the electro-optic effect), complemented by tensorial anisotropies expected to arise from the transition matrix elements. Furthermore, these anisotropies when considered in properly designed ER experiments would then provide information about the BZ location and interband topology of the transition under study.

The present study executes Phillips's suggestion and presents a general method for analyzing directional ER experiments in a manner which allows a direct correlation of the spectra to features of the band structure. It leads considerably beyond a previous study of Bottka and Rössler[8] and generalizes Aymerich and Bassani's treatment of a special case.[9] In goal and spirit, this study is similar to the symmetry analysis of piezoreflectance spectra recently presented by Sell and Kane.[10]

We introduce in Sec. II the basic definitions and assumptions of the symmetry analysis, justifying them by experimental facts. The correlation between the observed change in reflectance $\Delta R/R$ and the dielectric function is then presented.

We describe the change in reflectance by a product – or the sum of products – of two factors representing separately the two levels of anisotropies, tensorial and nontensorial.[7] The nontensorial electro-optic effect is assumed to depend only upon the modulating field. This dependence is strong, both in the magnitude and direction of the electric field. The tensorial factor representing the sampling of the field-perturbed dielectric function by the inci-

dent light depends, in general, upon both modulating field and direction of polarization, because the matrix element involves field-perturbed wave functions. The electric field dependence in this case is much weaker.

Being interested in the response of $\Delta R/R$ to changes in *direction*, not *magnitude*, of $\vec{F}$, we calculate the ratio of the ER response for two orthogonal polarizations of incident light. In general, this ratio will not depend strongly upon the magnitude of the electric field. Four special geometries of experimental interest are investigated in detail, assuming initially that the matrix elements are not affected by $\vec{F}$.

Direct transitions having principal axes along the three directions $\langle 100\rangle$, $\langle 111\rangle$, and $\langle 110\rangle$ of a cubic reciprocal lattice (having, respectively, fourfold, threefold, and twofold rotational symmetry) are considered, and the "ratio signature" is calculated for the four chosen geometries. A discrimination is shown to exist among the three transitions for electric fields along high-symmetry directions in the crystal, independent of the electro-optic mechanism.

We conclude Sec. II by generalizing some of the most important results to explicitly account for the effect of $\vec{F}$ on the transition matrix elements and on essential band degeneracies. Group-theoretical compatibility relations are employed to determine how the vectorial perturbation $\vec{F}$ reduces the symmetry of the point group associated with various BZ locations. The results give the selection rules and basis wave functions to be used in calculating field-perturbed matrix elements. Comparison of the signatures calculated here with those obtained under the field-free–matrix-element assumption leads to clear-cut experimental tests for the validity of that assumption. Signatures for transitions involving band degenerate levels are developed and suggestions for observing them in experiments are given. Section III presents experimental results as a test for these analytical predictions. Limitations of the current work and suggestions for extending the analysis are then presented in Sec. IV.

II. SYMMETRY ANALYSIS

A. General Considerations

We assume that the anisotropies in ER arise in the following manner. For transitions occurring off-center of the BZ, the incident polarized light samples individual branches of the star of $\vec{k}$ differently, depending upon the direction of the polarization vector $\vec{e}$ with respect to each branch $\vec{k}_i$. In cubic crystals with no applied field, the different sampling of $\vec{e}$ averages out after summing over the equivalent branches, and we obtain the usual polarization-independent isotropy. In the presence of the electric field perturbation the degeneracy of the star of $\vec{k}$ is lifted, each branch being affected differently by the applied field. This results in nonequivalent individual contributions to the total ER response. The different sampling of the polarized light weights the nonequivalent electro-optic effect at each branch $\vec{k}_i$, producing an observable anisotropy in ER. In principle, this anisotropy can result both from the field-affected matrix element and the electrooptic effect at each $\vec{k}_i$.

We incorporate these anisotropies into the symmetry analysis with the following "trial solution."[7] For points off-center of the BZ, the change induced in the dielectric function by the electric field, due to transitions at the ith branch of the star of $\vec{k}$, is described by a factor f_iQ_i, where f_i represents the matrix element as affected by the presence of $\vec{F}$, and Q_i is the dynamical factor describing the effect of $\vec{F}$ on the Hamiltonian of the crystal. We write the field-induced change in the imaginary part of the dielectric function as

$$\Delta\epsilon_2 = \sum_i f_i Q_i \,, \tag{1}$$

where we have summed over the branches of the perturbed star of $\vec{k}$. The removal of essential band degeneracies[11] can be accounted for by a second summation over the members of the multiplet, as discussed later.

The observed modulated response $\Delta R/R$ depends on the effect of $\vec{F}$ on ϵ_1 as well as ϵ_2. Therefore we must calculate $\Delta\epsilon_1$ via the Kramers-Kronig integral.[12] In field-free calculations of ϵ_1 we have to integrate over the entire spectrum; in calculating $\Delta\epsilon_1$ it suffices to integrate only over other structure in $\Delta\epsilon_2$ in the immediate vicinity of the frequency ω. This is a direct consequence of the localized nature of the structure.[13,14] For the same reason we can remove f_i from the integral, assuming it to be a slowly varying function of ω over the width of $\Delta\epsilon_2$. Consequently,

$$\Delta\epsilon_1(\omega) = \frac{1}{\pi\omega^2}\sum f_i P\int_{-\infty}^{\infty}\frac{d\omega'\omega'^2}{\omega'-\omega}\,Q_i(\omega') = \sum f_i Q_i' \,. \tag{2}$$

Finally, by adding the properly weighted contributions from field-induced changes of both optical constants we obtain the fractional change in reflectance[15,16]

$$\begin{aligned}(\Delta R/R)(\omega) &= \alpha(\omega)\Delta\epsilon_1(\omega) + \beta(\omega)\Delta\epsilon_2(\omega)\\ &= \sum_i f_i(\alpha Q_i' + \beta Q_i) = \sum_i f_i D_i \,,\end{aligned} \tag{3}$$

where we have defined D_i, the dynamical factor, as

$$D_i = \alpha Q_i' + \beta Q_i \,. \tag{4}$$

D_i will, in general, be a function of both the magnitude and the direction of the electric field:

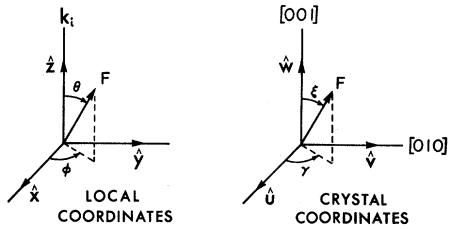

FIG. 1. (a) Polar coordinates θ and ϕ of the electric field vector $\vec{F}$ referred to the local frame of the ith reciprocal-lattice vector $\vec{k}_i$. The unit orthogonal components of the local frame are designated by $\hat{x}$, $\hat{y}$, and $\hat{z}$, with $\vec{k}_i \parallel \hat{z}$. (b) Polar components ξ and γ of the electric field vector $\vec{F}$ referred to the cubic crystal frame. The unit components $\hat{u}$, $\hat{v}$, and $\hat{w}$ are along the cube edges.

$D_i = D_i[F(\theta, \phi)]$, because of the anisotropy in the reduced mass. The polar angles ϕ and θ specify the orientation of $\vec{F}$ with respect to the principal direction $\vec{k}_i$ in the BZ contributing to the transition.

Since each $\vec{k}_i$ is generally intersected at a different angle by the external perturbation $\vec{F}$, it is useful to associate with each branch of the star of $\vec{k}$ in the first BZ a "local coordinate" system for which the origin coincides with the tip of the vector $\vec{k}_i$ and the z axis is parallel to $\vec{k}_i$. Figure 1(a) shows such a system along with the polar angles mentioned above. Note that for $\vec{k}_i$ of greater than twofold rotational symmetry D_i is independent of ϕ. Also, for cubic symmetries the following relations hold:

$$\frac{\partial D_i}{\partial \theta}(\theta, \phi) = 0 \quad \text{for } \theta = 0, \ \tfrac{1}{2}\pi \text{ for all } \phi \ , \tag{5}$$

$$\frac{\partial D_i}{\partial \phi}(\theta, \phi) = 0 \quad \text{for } \phi = 0, \ \tfrac{1}{2}\pi \text{ for all } \theta \ . \tag{6}$$

These relations will be useful later when we perform the summation over i in (3).

In Eq. (3), the factor f_i is the transition matrix element between states j and j', and is given in the dipole approximation by

$$f_i = |M_{jj'}|_i^2 = |\langle j|\vec{e}\cdot\vec{p}|\, j'\rangle|_i^2 \ , \tag{7}$$

where $\vec{p} = -i\hbar\vec{\nabla}$ is the momentum operator. When considering the orientation of $\vec{e}$ in the crystal with respect to each branch of $\vec{k}$, it is advantageous to decompose f_i along some convenient coordinate system. One logical choice would be to use the local coordinate system given in Fig. 1(a). In this system

$$(\vec{e}\cdot\vec{p})_i = e_{x_i} p_x + e_{y_i} p_y + e_{z_i} p_z \ , \tag{8a}$$

where

$$e_{x_i} = \vec{e}\cdot\hat{x}_i \ , \quad \text{etc.} \tag{8b}$$

$\hat{x}_i$ being the unit vector, from which

$$f_i = |X_i + Y_i + Z_i|^2 \ , \tag{9}$$

where, for example,

$$X_i = \langle j|\, e_{x_i} p_x|\, j'\rangle \ . \tag{10}$$

The quantity X_i is the matrix element for the transition at $\vec{k}_i$ if $\vec{e}$ is parallel to the x axis of the ith local coordinate system. The matrix element for any orientation of $\vec{e}$ can be expressed in terms of the components X_i, Y_i, and Z_i. This decomposition will be useful when we treat the case of field-free matrix elements in Sec. II B.

To treat the case of field-perturbed matrix elements, we will choose a new decomposition of f_i, namely, the component parallel to $\vec{F}$, denoted by P_i, and the component normal to $\vec{F}$, denoted by N_i. The components N_i and P_i are related to X_i, Y_i, and Z_i by a coordinate transformation corresponding to rotation through θ_i, the angle between $\vec{F}$ and $\vec{k}_i$.

The selection rules prescribed by the symmetry of the transition, the possible lowering of the symmetry by the field, and the actual strength of the transition are, in principle, all contained in (9). For example, if we apply an electric field $\vec{F}$ along $\vec{k}_i$, the symmetry of the wave functions associated with that particular branch of the star of $\vec{k}$ will not be lowered (unless the tip of $\vec{k}_i$ is at the surface of the BZ), and the field-free polarization selection rule will still apply. If $\vec{F}$ is not parallel to $\vec{k}_i$, the symmetry of the point $\vec{k}_i$ associated with the transition will be lowered, degeneracies may be lifted, and a new set of selection rules will apply. Some of the components of the matrix element which were previously zero will now be nonzero; the magnitude will depend on the strength and orientation of the field. As before, the following symmetry condition holds:

$$\frac{\partial X_i}{\partial \theta} = \frac{\partial Y_i}{\partial \theta} = \frac{\partial Z_i}{\partial \theta} = 0 \qquad \text{at } \theta = 0, \ \tfrac{1}{2}\pi \ . \tag{11}$$

The compatibility relations associated with the lowering of the symmetry by the field, the corresponding selection rules, and the form of the matrix elements will be discussed in detail in Sec. II C.

Having dealt formally with the factors f_i and D_i, which we have assumed to be the two components of ER response, we now must arrive at a reliable method for experimentally extracting the symmetry information contained therein. We will assume an experimental geometry in which the orientation of $\vec{F}$ may be varied with respect to the crystal axes and call it the trajectory of $\vec{F}$. Figure 1(b) shows the polar angles ξ and γ of $\vec{F}$ with respect to the

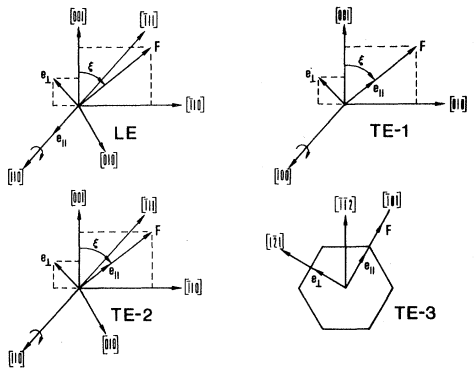

FIG. 2. Trajectories of the electric field $\vec{F}$ in crystal coordinates. The polarization vector $\vec{e}$ perpendicular or parallel to the field $\vec{F}$ is designated by TE, and $\vec{e}$ perpendicular or parallel to the axis of rotation by LE.

crystal axes; these two angles become the independent variables of the experiment. In this study we will consider only trajectories in which the incident light direction is normal to the plane of reflection and the modulating field $\vec{F}$ is parallel or normal to the incident light beam. These are classified in experiments as the longitudinal (LE) and transverse (TE) geometries, respectively.

Four trajectories will be treated in detail; these are shown in Fig. 2. In the LE trajectory, the sample rotates about the [110] direction[17]; the azimuth γ is constant at $\frac{3}{4}\pi$, and the trajectory parameter ξ (measured from [001]) defines the orientation of $\vec{F}$ in the plane of rotation. The light incidence is parallel to $\vec{F}$ and lies in the plane of rotation; reference directions of $\vec{e}$ are normal and parallel to the axis of rotation. In the LE trajectory, $\vec{e}$ is always normal to $\vec{F}$. In the other three trajectories, $\vec{F}$ lies in the reflecting plane[6]; these planes are (100), denoted by TE-1; (110), denoted by TE-2; and (111), denoted by TE-3. The reference polarizations are normal and parallel to $\vec{F}$. For TE-1 and TE-2, ξ defines the orientation of $\vec{F}$ relative to [001] in the reflecting plane; the azimuth γ is fixed at 0 and $\frac{3}{4}\pi$, respectively. The only difference between LE and TE-2 is the manner in which the individual D_i's are sampled by the polarization vector; each D_i is identical for these two trajectories.

Over these four trajectories we will evaluate the "polarization ratio signature," defined by

$$S(\xi, \mathrm{LE}) = \frac{\Delta R(\vec{e}_\perp[110])/R_\perp}{\Delta R(\vec{e}_\parallel[110])/R_\parallel} = \frac{\Delta R_\perp(\vec{e}_\perp[110])}{\Delta R_\parallel(\vec{e}_\parallel[110])} \quad (12)$$

for the LE trajectory, where [110] is the axis of rotation, and

$$S(\xi, \mathrm{TE}) = \frac{\Delta R(\vec{e}_\perp\vec{F})/R_\perp}{\Delta R(\vec{e}_\parallel\vec{F})/R_\parallel} = \frac{\Delta R_\perp(\vec{e}_\perp\vec{F})}{\Delta R_\parallel(\vec{e}_\parallel\vec{F})} \quad (13)$$

for the TE trajectories. We choose this signature because in forming the ratio (12) or (13) as we vary ξ, we "divide out" variations in $|\vec{F}|$ along the trajectory[17]; any observed change in ER response as we rotate $\vec{e}$ at fixed ξ will have its basis in the symmetry of the transition. The correlation between experiments and Eqs. (12) and (13) is made by recording the magnitude of the ER structure as a function of ξ and polarization direction.

We assume in (12) and (13) that the reflectance R is polarization independent, implying an unstrained cubic system. The extension to noncubic cases is tedious but straightforward.

B. Field-Free Matrix Element

We apply Eqs. (3), (12), and (13) to the principal BZ directions Δ and Λ, assuming initially that the matrix elements of the field-free crystal provide an adequate description of the optical sampling in the presence of $\vec{F}$,[7,12] and that the bands involved in the transition are nondegenerate.

Two simplifications result from the assumption of field-free matrix elements. First, the matrix-element *components* (9) are no longer functions of $\vec{F}$ and are thus identical for each branch of the star of $\vec{k}$ (although the individual f_i will be different because the angles between $\vec{e}$ and each $\vec{k}_i$ are different). Second, the principal axes Δ and Λ remain fourfold and threefold rotationally symmetric, respectively; the matrix-element components (9) can thus be simplified because $X_i = Y_i$. Therefore we introduce the "radial component" $R_i = 2X_i$.

Tables I and II summarize the main steps in calculating the ratio signatures for $\vec{F}$ along high-symmetry directions in the crystal. Table I shows the equivalence relations among the D_i's for each transition; the angles in parentheses indicate the angle between $\vec{F}$ and $\vec{k}_i$; the parameter ξ and the index i identify $\vec{F}$ and $\vec{k}_i$ in the crystal frame [Fig. 1(b)], respectively. Table II exemplifies the matrix element decomposition [Eqs. (8)–(10)] for a Δ transition in the TE-1 trajectory; the two reference polarizations $\vec{e}_\perp$ and $\vec{e}_\parallel$ are expressed in terms of the unit vectors of the crystal coordinate system [Fig. 1(b)] and then Eqs. (8)–(10) are followed through for the six branches of the star of $\vec{k}$.

Table III presents the results of calculating S via (12) and (13) for transitions of Λ and Δ symmetry; these are the basic results of our symmetry analysis. Table III contains the following information:

(i) There are values of trajectory parameter ξ for which $S = 1$; in other words, the ER response is identical for both reference polarizations. These $S = 1$ values fall into two categories. (a) In the LE trajectory, $S = 1$ for Δ and Λ symmetries (the same is true for any symmetry) with $\vec{F} \parallel [001]$ or $[\bar{1}11]$ ($\xi = 0°$ or $54°\,44'$); these unit entries merely reflect the cubic structure of the crystal and make no dis-

TABLE I. Equivalence among the dynamical factors D_i when the electric field is along the principal symmetry directions in the crystal. The angles in parentheses correspond to θ and ϕ shown in Fig. 1(a). The trajectories are defined in Fig. 2.

Trajectory	Trajectory parameter ξ	Field direction	Δ	Λ	Σ
TE-1	0°	[001]	$D_1=D_2=D(90°)$; $D_3=D(0°)$	All $D_i=D(54°44')$	$D_1=D_2=D(90°, 90°)$ $D_3=D_4=D_5=D_6=D(45°, 45°)$
	45°	[011]	$D_1=D(90°)$; $D_2=D_3=D(45°)$	$D_1=D_2=D(35°16')$ $D_3=D_4=D(90°)$	$D_1=D_2=D_3=D_4=D(60°, 60°)$ $D_5=D(0°, 90°)$; $D_6=D(90°, 0°)$
TE-2, LE	0°	[001]	$D_1=D_2=D(90°)$; $D_3=D(0°)$	All $D_i=D(54°44')$	$D_1=D_2=D(90°, 90°)$ $D_3 D_4=D_5=D_6=D(45°, 45°)$
	54°44′	[$\bar{1}$11]	All $D_i=D(54°44')$	$D_1=D_3=D_4=D(70°32')$ $D_2=D(0°)$	$D_1=D_3=D_6=D(90°, 35°16')$ $D_2=D_4=D_5=D(35°16', 90°)$
	90°	[$\bar{1}$10]	$D_1=D_2=D(45°)$; $D_3=D(90°)$	$D_1=D_3=D(90°)$ $D_2=D_4=D(35°16')$	$D_1=D(90°, 0°)$; $D_2=D(0°, 90°)$ $D_3=D_4=D_6=D(60°, 60°)$

tinction among transitions of different symmetry. This is an inherent feature of the LE trajectory, in which both reference polarizations are perpendicular to $\vec{F}$. If $\vec{F}$ is parallel to a direction of greater than twofold symmetry, the symmetry of the plane normal to $\vec{F}$ is not altered and the dipole matrix element remains independent of the angle of polarization in that plane. This result also carries over to the case of field-perturbed matrix elements, as discussed in Sec. IIC. (b) In the TE-1 and TE-2 trajectories, on the other hand, the $S=1$ entries now occur for different values of ξ according to whether the transition is of Λ or Δ symmetry. There are two independent signatures which allow unambiguous assignments: $S(0°, \text{TE-1})=1$ for Λ but not Δ, while $S(45°, \text{TE-1})=1$ for Δ but not Λ. Similar discrimination holds for TE-2.

(ii) Referring to Table I, we see that the unit entries $S(0°, \Lambda, \text{TE-1})$, $S(0°, \Lambda, \text{TE-2})$, $S(54°44', \Delta, \text{TE-2})$ result from the equivalence of the D_i's; the other unit entries result from the equivalence of matrix-element components for both reference polarizations.

(iii) The values of $S(90°, \text{LE})$ and $S(90°, \text{TE-2})$ are identical for Δ; the same is not true for Λ. We also have the trivial result that $S(0°, \text{TE-1}) = S(0°, \text{TE-2})$ for any symmetry.

The nonunit entries in Table III also contain symmetry information, but require some knowledge of $D(\theta)$ and the matrix-element components R and Z before they can be utilized. Or, turning the statement around, having experimental results corresponding to the entries in Table III, we should be able to extract information about $D(\theta)$, R, and Z. We will discuss this in detail in Sec. III.

As an example, we now consider a specific se-

TABLE II. The projection of the polarization vector $\vec{e}$ along the local coordinates of the star of $\vec{k}$ having symmetry Δ. $\vec{e}$ is given in terms of the unit vectors of the crystal coordinate [Fig. 1(b)] for cases perpendicular ($\vec{e}_\perp$) and parallel ($\vec{e}_\parallel$) to the electric field; $\vec{F}$ rotates in the TE-1 trajectory. The matrix elements are expressed in terms of Z, the projection of $\vec{e}$ along the axis $\vec{k}_i$, and R in the plane perpendicular to $\vec{k}_i$. The primed indexes refer to the stars of $\vec{k}_i$ diagonally opposite to the unprimed ones. The upper sign refers to the unprimed, the lower sign to the primed index of i.

	$\vec{e}_\perp=-\hat{v}\cos\xi+\hat{w}\sin\xi$			$\vec{e}_\parallel=\hat{v}\sin\xi+\hat{w}\cos\xi$		
i	1, 1′	2, 2′	3, 3′	1, 1′	2, 2′	3, 3′
$\vec{e}\cdot\hat{x}_i$	$-\cos\xi$	0	0	$\pm\sin\xi$	0	0
$\vec{e}\cdot\hat{y}_i$	$\sin\xi$	$\sin\xi$	$-\cos\xi$	$\cos\xi$	$\cos\xi$	$\sin\xi$
$\vec{e}\cdot\hat{z}_i$	0	$\pm\cos\xi$	$\pm\sin\xi$	0	$\pm\sin\xi$	$\pm\cos\xi$
$\vec{e}_{Ri}$	1	$\sin\xi$	$\cos\xi$	1	$\cos\xi$	$\sin\xi$
$\langle j'\lvert\vec{e}\cdot\vec{p}\rvert j\rangle_i$	R	$R\sin\xi\mp Z\cos\xi$	$R\cos\xi\pm Z\sin\xi$	R	$R\cos\xi\pm Z\sin\xi$	$R\sin\xi\pm Z\cos\xi$

TABLE III. Polarization ratio signature for Δ and Λ symmetries, with the electric field along high-symmetry directions in the different trajectories. The results are given in terms of the dynamical factor D_i and the components of the matrix element parallel (Z) and perpendicular (R) to the nonequivalent principal directions of $\vec{k}_i$. The subscript angle refers to the angle between the electric field and the star of $\vec{k}_i$. These results are valid when the matrix elements of the unperturbed system are applicable.

Trajectory	Trajectory parameter ξ	Field direction	Polarization ratio signature: Δ symmetry	Polarization ratio signature: Λ symmetry
LE	0°	[001]	1	1
	54°44′	[$\bar{1}$11]	1	1
	90°	[$\bar{1}$10]	$\dfrac{2D_{45°}R^2+D_{90°}Z^2}{(D_{45°}+D_{90°})R^2+D_{45°}Z^2}$	$\dfrac{(D_{35°16'}+D_{90°})(2R^2+Z^2)}{3D_{35°16'}R^2+D_{90°}(R^2+2Z^2)}$
TE-1	0°	[001]	$\dfrac{(D_{0°}+D_{90°})R^2+D_{90°}Z^2}{2D_{90°}R^2+D_{0°}Z^2}$	1
	45°	[011]	1	$\dfrac{(3D_{35°16'}+D_{90°})R^2+2D_{90°}Z^2}{(D_{35°16'}+3D_{90°})R^2+2D_{35°16'}Z^2}$
TE-2	0°	[001]	$\dfrac{(D_{0°}+D_{90°})R^2+D_{90°}Z^2}{2D_{90°}R^2+D_{0°}Z^2}$	1
	54°44′	[$\bar{1}$11]	1	$\dfrac{(3D_{0°}+5D_{70°32'})R^2+4D_{70°32'}Z^2}{8D_{70°32'}R^2+(3D_{0°}+D_{70°32'})Z^2}$
	90°	[$\bar{1}$10]	$\dfrac{2D_{45°}R^2+D_{90°}Z^2}{(D_{45°}+D_{90°})R^2+D_{45°}Z^2}$	$\dfrac{(D_{35°16'}+D_{90°})(2R^2+Z^2)}{(D_{35°16'}+3D_{90°})R^2+2D_{35°16'}Z^2}$
TE-3	•••	[$\bar{1}$01]	$\dfrac{(5D_{45°}+D_{90°})R^2+(D_{45°}+2D_{90°})Z^2}{3(D_{45°}+D_{90°})R^2+3D_{45°}Z^2}$	$\dfrac{(7D_{35°16'}+5D_{90°})R^2+(2D_{35°16'}+4D_{90°})Z^2}{(3D_{35°16'}+9D_{90°})R^2+6D_{35°16'}Z^2}$

lection rule, namely, $R=R_0$, $Z=0$ (that is, $\vec{e}\perp\vec{k}_i$ allowed, which is common in diamond and zinc-blende lattices), and a simple model for $D(\theta)$. We assume direct transitions in a one-electron band structure, in which the field perturbation of ϵ_2 is characterized by the curvature of the interband energy surface along the field direction; if $\vec{F}$ is along a direction of zero curvature, we require $D(\theta)=0$. This can be formalized by writing

$$D(\theta)\sim\pm F_x^2(\theta)/\mu_x\pm F_y^2(\theta)/\mu_y\pm F_z^2(\theta)/\mu_z . \quad (14)$$

μ_x, μ_y, and μ_z are the components of the reduced masses in the local coordinate. The signs are chosen to represent the signs of the curvatures along the local coordinate axes, Fig. 1(a); as usual, the z component is parallel to $\vec{k}_i$. Equation (14) is rigorously true at low[18] $|\vec{F}|$ because the line shape of $\Delta R/R$ is independent of the magnitude of $\vec{F}$. If all signs are identical, the interband energy separation at $\vec{k}_i$ is an extremum; if not, we have a saddle point. The four possible cases are classified[13] by M_l, where l is the number of negative masses in (14). For BZ directions of greater than twofold rotational symmetry, $\mu_x=\mu_y$ and we define $c\equiv\mu_x/\mu_z$. For $M_1(+)$ and $M_2(-)$ types, we have

$$D(\theta)\sim\pm(\sin^2\theta-c\cos^2\theta) , \quad (15)$$

whereas for $M_0(+)$ and $M_3(-)$,

$$D(\theta)\sim\pm(\sin^2\theta+c\cos^2\theta) . \quad (16)$$

These functions are plotted in Fig. 3 for several values of c. Note that they satisfy the symmetry requirements (5).

Equations (15) and (16) have the same symmetry properties as the generalized Franz-Keldysh theory.[12,19] For a saddle point (M_1, M_2), $D(\theta_c)=0$, where $\tan^2\theta_c=c$; physically this means that there is no response if $\vec{F}$ is along a direction of infinite interband mass. Furthermore, $D(\theta)$ changes sign as $\vec{F}$ crosses θ_c; this corresponds to the change in spectral line shape from one to the other of the electro-optic functions[12] as $\vec{F}$ crosses the cone defined by zero curvature of the interband energy surface.

We have computed $S(\xi)$ for Δ and Λ in the TE-1, TE-2, and LE trajectories (a transformation from θ to ξ is involved); the results are shown in Fig. 4 for transitions of M_1 or M_2 type. Since M_1 differs from M_2 (and M_0 from M_3) only in the sign of each of the D_i's, the particular signature we have chosen does not distinguish between the two types of saddle

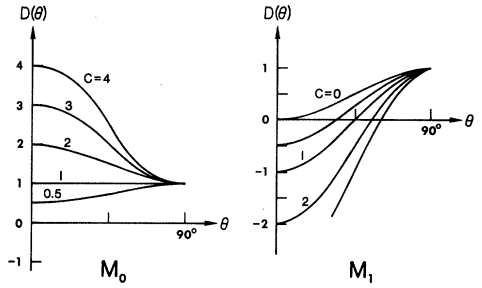

FIG. 3. A model electro-optic mechanism $D(\theta)$ as a function of the angle θ between the $\vec{F}$ and the principal axis $\vec{k}$, given by Eqs. (15) and (16). The parameter c is the reduced mass ratio, $c=\mu_x/\mu_z$.

point (or the two types of extremum). The TE-1 and TE-2 trajectories in Fig. 4 yield an unambiguous choice between Δ and Λ symmetries; in principle, one can determine both the symmetry and mass ratio c from either trajectory. The LE signature, shown in the bottom of Fig. 4, is ambiguous with respect to the mass ratio: a Δ transition with $c \ll 1$ is indistinguishable from a Λ transition with $c \gg 1$.

Note that the $S(\xi)$ curves of Fig. 4 go through certain high-symmetry values of ξ with zero slope, as required by the symmetry condition (5) on $D(\theta)$. For the LE trajectory, it can be shown that the combination $S=1$, $dS/d\xi = 0$ can only occur at $\xi = 0$, regardless of the symmetry of the transition.

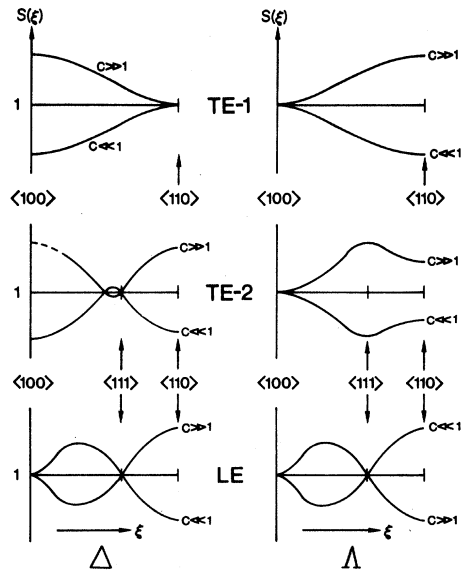

FIG. 4. General signature pattern for the different trajectories for Δ and Λ symmetries. Equation (15) was used for $D(\theta)$ with the selection rule $Z=0$.

C. Effect of $\vec{F}$ on Matrix Elements and Band Degeneracies

We now consider alterations to the signatures of Table III which result from field-dependent matrix elements and the removal of essential band degeneracies. We will employ results from group theory in which the electric field vector $\vec{F}$ is the symmetry determining axis, so it becomes convenient to decompose the matrix element f_i into components N_i, $\vec{e}$ normal to $\vec{F}$, and P_i, $\vec{e}$ parallel to $\vec{F}$:

$$f_i = (N_i + P_i)^2 , \qquad N_i = |\langle j|\, \vec{e}_\perp \cdot \vec{p}\, |j'\rangle| ,$$

$$P_i = |\langle j|\, \vec{e}_\parallel \cdot \vec{p}\, |j'\rangle| , \tag{17}$$

where the subscript on $\vec{e}$ refers to its orientation with respect to $\vec{F}$.

In general, the effect of $\vec{F}$ on the unperturbed system (described by the group of the star of $\vec{k}$) will be to reduce the symmetry; the new system will have to be compatible with the previous symmetry. The consistency between the old and new system is given by compatibility tables (for example, Ref. 20). To illustrate, consider the point Γ in the BZ which has the symmetry of the full cube, i.e., the point group O_h. By applying $\vec{F}$ to this system, we establish a symmetry axis, and instead of O_h we will have $\vec{F} \parallel \langle 100\rangle$, $\langle 111\rangle$, and $\langle 110\rangle$ compatible with C_{4v}, C_{3v}, and C_{2v}, respectively. In Fig. 5, we show the effect of $\langle 100\rangle$ and $\langle 111\rangle$ fields on the Γ_7^-, Γ_8^+, and Γ_7^+ levels in the diamond lattice; the new selection rules in the presence of $\vec{F}$ are indicated. The Γ_8^+ degeneracy is removed for any orientation of $\vec{F}$; the ordering of the split levels is that suggested by Enderlein *et al.*[11]

For points off-center of the BZ, we must consider three cases. (i) At an interior point, $\vec{F} \parallel \vec{k}_i$ does not affect the symmetry, although the actual amplitudes of the wave functions may change. If the field-free matrix elements are $R=R_0$ and $Z=0$, the new values

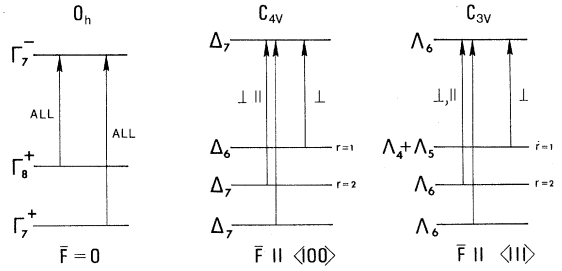

FIG. 5. Schematic representation of the point group O_h and the energy levels Γ_7^+, Γ_8^+, and Γ_7^-. The compatible symmetries are shown as the electric field is applied parallel to $\langle 100\rangle$ and $\langle 111\rangle$. The polarization selection rules are referenced to the electric field direction, either $\vec{e} \parallel \vec{F}$ or $\vec{e} \perp \vec{F}$. The Γ_8^+ degeneracy is removed by $\vec{F}$; the lower-energy member of the $\Gamma_8^+ \rightarrow \Gamma_7^-$ doublet is only allowed for $\vec{e} \perp \vec{F}$.

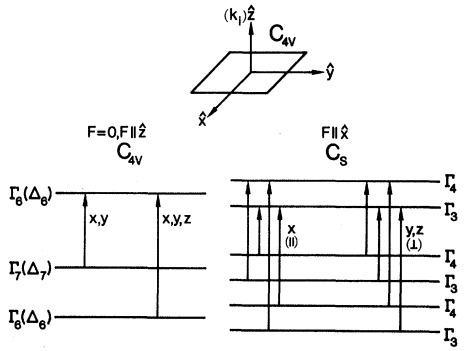

FIG. 6. Schematic representation of the point group C_{4v} and the energy levels $\Delta_6(\Gamma_6)$, $\Delta_7(\Gamma_7)$ of the diamond lattice involved in the transition. The compatible symmetries are shown as the electric field is applied parallel or perpendicular to the Δ axis. In labeling energy levels, we give the usual band-structure notation first, then the notation of Ref. 20 in parentheses.

with $\vec{F} \parallel \vec{k}_i$ will be $R = R$ and $Z = 0$ (or, in the new decomposition scheme, $N = N$ and $P = 0$). The selection rules for representative Δ and Λ transitions with $\vec{F} \parallel \vec{k}_i$ ($\vec{F} \parallel \hat{z}$) are shown in the left-hand sides of Figs. 6 and 7. (ii) For points on the zone face, $\vec{F} \parallel \vec{k}_i$ removes the inversion symmetry of the plane perpendicular to $\vec{k}_i$ but does not affect the rotational symmetry. In the absence of essential band degeneracies, the selection rules simply revert to those of an interior point having the same rotational symmetry (for example, $\vec{F} \parallel \vec{k}_i$ reduces the L-point selection rules to those of the Λ direction in diamond). If such degeneracies do exist, they will be lifted by $\vec{F} \parallel \vec{k}_i$. This is shown for the degenerate X_5 level in diamond in the center diagram of Fig. 8. (iii) For $\vec{F} \perp \vec{k}_i$, the rotational symmetry of threefold and fourfold $\vec{k}_i$ will be lowered, degeneracies will be lifted, and new selection rules will apply. This is shown schematically in the right-hand diagrams of Figs. 6–8 for Δ, Λ, and X, respectively. The group-theoretical basis is given explicitly in Refs. 20–23.

Certain conclusions about the signature can be drawn immediately by considering how $\vec{F}$ in certain directions affects the symmetry of the crystal. In the LE trajectory the polarization vector is always perpendicular to the electric field perturbation, and for $\vec{F}$ parallel to $\langle 100 \rangle$ or $\langle 111 \rangle$ the plane of polarization remains fourfold and threefold rotationally symmetric, respectively. Since we consider dipole transitions only, we conclude that the $S = 1$ points in the LE trajectory (Table III) are still valid. This will not be generally true for the TE trajectory since $\vec{e}$ samples parallel and perpendicular to the field, or perturbation, axis. Thus the TE signatures should provide the most straightforward evidence for degeneracy and matrix-element effects.

As an example, consider $S(0°, \Delta, \text{TE-1})$, where $\vec{F} \parallel [001]$ and $\vec{e}$ rotates in the (100) plane. One branch of the star has $\vec{F} \parallel \vec{k}_i$ (or $\vec{F} \parallel \hat{z}$ in Fig. 6) and the group $\vec{k}_i$ is still C_{4v}. For this star, components of the matrix element that were zero in the unperturbed case are still zero; the others might not have the same magnitude. The other two branches have $\vec{F} \perp \vec{k}_i$ ($\vec{F} \parallel \hat{x}$ or $\hat{y}$ in Fig. 6); the symmetry is reduced to C_s and the time-reversal degeneracy of both initial and final states is lifted. The exact nature of the matrix element depends upon the specific Δ transition being considered as well as the orientation of $\vec{e}$. The transition $\Delta_7 \rightarrow \Delta_6$ in the diamond lattice has $R = R_0$, $Z = 0$ in the absence of $\vec{F}$, so the branch with $\vec{F} \parallel \vec{k}_i$ has $N = N$ and $P = 0$ in the presence of $\vec{F}$. For the other two branches, Δ_7 and Δ_6 both

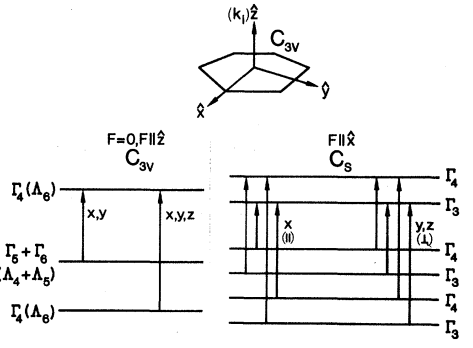

FIG. 7. Schematic representation of the point group C_{3v} and the energy levels $\Lambda_6(\Gamma_4)$, $\Lambda_4(\Gamma_5) + \Lambda_5(\Gamma_6)$ of the diamond lattice involved in the transition. The compatible symmetries are shown as $\vec{F}$ is applied parallel and perpendicular to Λ.

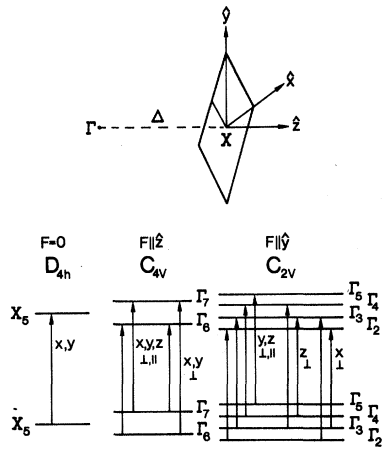

FIG. 8. Schematic representation of the X point at the BZ face in the diamond lattice. The compatible symmetries along with the selection rules for the electric field along different directions in the crystal are shown.

split into $\Gamma_3+\Gamma_4$ (using the notation of Ref. 20), and the selection rules indicated in Fig. 6 lead to

$$N^2(C_s)=\left|\langle\Gamma_3|\vec{e}_\perp\cdot\vec{p}|\Gamma_3\rangle+\langle\Gamma_4|\vec{e}_\perp\cdot\vec{p}|\Gamma_4\rangle\right|^2, \quad (18)$$

$$P^2(C_s)=\left|\langle\Gamma_3|\vec{e}_\parallel\cdot\vec{p}|\Gamma_4\rangle+\langle\Gamma_4|\vec{e}_\parallel\cdot\vec{p}|\Gamma_3\rangle\right|^2. \quad (19)$$

The signature (13) for this transition contains matrix elements appropriate to C_{4v} for the branch with $\vec{F}\parallel\vec{k}_i$ and to C_s for the two branches with $\vec{F}\perp\vec{k}_i$, given in (19) above.

Let us now consider what happens to the $S=1$ entries for the TE trajectories in Table II which were based on the equivalence of the D_i ($\vec{F}\parallel\langle 100\rangle$ for Λ, $\vec{F}\parallel\langle 111\rangle$ for Δ). In both of these cases, $\vec{F}$ makes an angle of 54° 44′ with each $\vec{k}_i$. The symmetry cannot be reduced below C_s (the group of C_s consists of the identity and a reflection using the notation of Ref. 20) so the selection rules for $\vec{F}$ oblique to $\vec{k}_i$ are identical to $\vec{F}\perp\vec{k}_i$, as shown on the right in Figs. 6 and 7. The signature in both cases is simply the ratio of field-perturbed matrix elements with $\vec{e}\perp$ and $\parallel\vec{F}$:

$$S=N^2(C_s)/P^2(C_s),$$

where the matrix elements are given in (18) and (19). This new value is not unity; it must approach unity as $|\vec{F}|$ is reduced in the experiment.

Finally, we treat the case in which the transitions originate from degenerate bands, namely, the Γ point in the diamond structure. We retain the product f_iD_i for the ER response, where now the subscript labels the degenerate levels; we assume that the total ER response arises as a superposition of contributions from the degenerate levels. In experiments, the effect of $\vec{F}$ is not to split observed peaks, as in piezospectroscopy or the Stark effect of atoms, but simply to introduce anisotropies of the peak size as the polarizer is rotated. As in the case of $\vec{k}$-star degeneracies, polarization anisotropies in ER will be expected only if the degenerate levels have different effective masses and the selection rules show polarization discrimination as $\vec{e}$ samples parallel or perpendicular to $\vec{F}$, i.e., $f(\vec{e}\perp\vec{F})\neq f(\vec{e}\parallel\vec{F})$. In Fig. 5, the transition connecting the degenerate Γ_8^+ level ($r=1,2$) and Γ_7^- will have the following signatures:

$$S(\mathrm{LE},\ 90^\circ)=\frac{f_1(\vec{e}\parallel[001]\perp\vec{F})D_1+f_2(\vec{e}\parallel[001]\perp\vec{F})D_2}{f_1(\vec{e}\parallel[110]\perp\vec{F})D_1+f_2(\vec{e}\parallel[110]\perp\vec{F})D_2} \quad (20)$$

for the LE trajectory, and

$$S(\mathrm{TE})=\frac{f_1(\vec{e}\perp\vec{F})D_1+f_2(\vec{e}\perp\vec{F})D_2}{f_1(\vec{e}\parallel\vec{F})D_1+f_2(\vec{e}\parallel\vec{F})D_2} \quad (21)$$

for the TE trajectory.

From the selection rules in Fig. 5, it is seen that ER in the LE trajectory will not show polarization anisotropy unless the energy surface surrounding the critical point is nonparabolic. In the TE trajectory, polarization dependence is possible, provided the effective masses of the degenerate levels are different from one another, and again, that $f(\vec{e}\perp\vec{F})\neq f(\vec{e}\parallel\vec{F})$.

In the case of band degeneracies for points off-center of the BZ (like the X point in diamond) polarization anisotropies would always be expected, the total contribution coming both from the star of $\vec{k}$ and band degeneracy. Thus, for the X_5-X_5 transition shown in Fig. 7, we would expect a polarization dependence even when $\vec{F}\parallel\langle 111\rangle$, i.e., the sum in Eq. (3) would reduce to a sum over the four levels of the doubly degenerate X_5 states. Detailed treatments of field effects on Γ- and X-point degeneracies are given in Refs. 11 and 24.

III. DISCUSSION

In this section, we present guidelines for applying the results of Sec. II to experiment. Evidence to support the present treatment will be given.

The first experiment should seek to confirm the field-free-matrix-element assumption, namely, by measuring S as a function of $|\vec{F}|$. A constant signature over a range of $|\vec{F}|$ would indicate that the results of Sec. II B apply. The following order of investigation would then be appropriate:

(i) The TE entries of Table III can be applied directly to obtain the principal axis of the transition. A Λ transition will produce no polarization dependence ($S=1$) for $\vec{F}\parallel\langle 100\rangle$ in either the TE-1 or TE-2 trajectory, whereas a Δ transition will exhibit $S=1$ for $\vec{F}\parallel\langle 111\rangle$ in the TE-2 trajectory, or $\vec{F}\parallel\langle 110\rangle$ in TE-1. The first three of these unit entries are based upon the complete equivalence of the various D_i's (see Table I), and are thus totally independent of the details of the electrooptic mechanism. If none of these experiments produce $S=1$ and if the field-free-matrix-element assumption has been verified, then the symmetry of the transition must be twofold or less. If $S(\mathrm{TE})=1$ for any orientation of $\vec{F}$, a Γ transition is indicated.

(ii) If experiment does provide a clear-cut distinction between Δ and Λ, then we can consider their specific polarization selection rules and make measurements on the remaining configurations in Table III. These give three independent equations in the three unknowns $D(0^\circ)$, $D(45^\circ)$, and $D(90^\circ)$ for Δ, and five equations in four unknowns $D(0^\circ)$, $D(35^\circ 16')$, $D(70^\circ 32')$, and $D(90^\circ)$ for Λ. Knowing $D(\theta)$ for three values of θ would allow determination of the components of the effective-mass tensor at the BZ point where the transition occurs. To do this, a model for $D(\theta)$ must be assumed; the one applied in Sec. II B is a possibility.

(iii) If we have no prior knowledge of the selection

rules, but we have found the principal axis of the transition from the $S=1$ values, experiments performed on the other trajectories in Table III still produce at least three equations in the three ratios $D(0°)/D(90°)$, $D(45°)/D(90°)$, and R^2/Z^2, in the case of a Δ transition. The value of the ratio R^2/Z^2 indicates the symmetry of the wave functions associated with the initial and final states of the transition; in other words, the value of R^2/Z^2 tells us specifically which Δ transition we are observing. If the system of simultaneous equations can only be satisfied by $R^2/Z^2 \gg 1$, then $Z=0$ and R is finite, which means the transition is only allowed for $\vec{e} \perp \vec{k}_i$. If R^2/Z^2 has some finite value, we are provided with an experimental check of calculated matrix elements for transitions in which both polarizations are allowed. Information of this kind can be used to verify the ordering of the various energy bands in calculated band structures.

(iv) As pointed out in Sec. II, the LE trajectory does not provide clear-cut information about the symmetry of transition. However, it can be used to measure S as a continuous function of ξ,[17] which is not presently feasible in TE experiments. The behavior of $(dS/d\xi)(\xi)$ provides an additional test of the validity of the model in Sec. II B (see Figs. 3 and 4). For example, one of the results was $dS/d\xi=0$ only for $\xi=0°$ and 90° (due to cubic symmetry). If, in addition, an LE experiment yields $(dS/d\xi) \times(54°\,44')=0$, or additional values of ξ where $S=1$, then the assumptions leading to Fig. 4 must be reexamined.

In the event that S is a function of $|\vec{F}|$, we can still indirectly utilize the TE unit entries to establish the principal axis of the transition. For example, if with $\vec{F} \parallel \langle 100 \rangle$ S extrapolates to unity at $|\vec{F}|=0$, we would be correct in assigning the transition to the Λ direction in the BZ; furthermore, $S(|\vec{F}|)$ is a direct measure of the range of validity of the weak-field approximation.

A variation of S with $|\vec{F}|$ would be analogous to a stress deformation potential, in which interband mixing by $\vec{F}$ contributes to the anisotropy of $\Delta R/R$. The polarization dichroism for each $|\vec{F}|$ would indicate the presence of "Stark" splitting in the bands. Normally, such splitting would be too small to be observed in solids; although the splitting would increase with $|\vec{F}|$, the collision broadening of the electro-optic structure would make observation of the splitting difficult. An alternative approach would be to infer "Stark splitting" from the difference of linewidth of the electroreflectance signal for the two reference polarizations.[24]

Such effects would probably be more pronounced in the TE trajectories, in which the perturbed matrix element is sampled both parallel and perpendicular to the perturbation direction. This does *not* imply that the LE trajectory will not exhibit field-dependent signatures as well, since N and P can be expressed in terms of R and Z (or X, Y, and Z if the rotational symmetry is reduced by $\vec{F}$). The interpretation would be more cumbersome, and the geometry favors the TE trajectories if such information is sought.

As seen from Sec. II, the ratio N/P is extractable from signatures where the field orientation is such that all D_i's are equivalent. This is the case for $\vec{F} \parallel \langle 111 \rangle$ for Δ, $\vec{F} \parallel \langle 100 \rangle$ for Λ and any direction of $\vec{F}$ for Γ. These give information not only about the levels in the degenerate set which contribute to the transition, but also indicate to what extent such degeneracies are lifted by the field.

Several recent papers provide experimental verification for some of the analytical results; we discuss them briefly here.

Polarization-dependent surface-barrier ER spectra on (110) planes [corresponding to $S(\mathrm{LE}, 90°)$] have been reported for Si[4] and Ge.[25] In neither case was the multibranch nature of the transitions accounted for. Variation of $\bar{e}$ in the latter case was done primarily to unravel overlapping structures believed to be present between 2.0 and 3.6 eV.

Recently we reported measurements on [110] axis Ge cylinders,[17] corresponding to the complete ξ dependence of $S(\mathrm{LE})$. The data for the E_1, $E_1+\Delta_1$ doublet (2.1 and 2.3 eV) were in accord with Fig. 4, indicating a value of $c<1$ assuming a Λ transition. The three components of the E_2 structure (4.4 eV) all exhibited different $S(\xi)$ behavior; we tentatively concluded the existence of more than one transition having nearly equal energies but different symmetry character.

High-resistivity germanium suitable for transverse electroreflectance was obtained by γ-ray compensation; preliminary data demonstrated the power of the TE analytical results.[26] With field strengths well below 10^4 V/cm, values of S for the E_1, $E_1+\Delta_1$ doublet were obtained which clearly established the Λ symmetry of these transitions. Forman, Aspnes, and Cardona[27] prepared semi-insulating Si by gold compensation; their TE spectra of the 3.4-eV complex were polarization dependent for all three principal orientations of $\vec{F}$ (one component of the structure had $S=1$ with $\bar{F} \parallel [110]$). From Table III, it is clear that transitions of Λ, Δ, and Γ symmetry do not contribute to this structure, so the location of the elusive[1] $\Gamma_{25'}-\Gamma_{15}$ fundamental direct gap remains unsolved.

Matrix element and degeneracy effects were demonstrated by detailed TE measurements on the E_0 direct gap of Ge.[24] For any orientation of $\vec{F}$, the period of characteristic Airy oscillations was found to be greater with $\vec{e} \parallel \vec{F}$ than $\vec{e} \perp \vec{F}$. A consistent interpretation was obtained by invoking the incipient (unresolved) removal of the light-heavy hole degeneracy as shown in Fig. 5; the total response be-

came the sum of light and heavy hole contributions, each represented by a different spectral function $D(\vec{F})$. The polarization-dependent weighting of these contributions was obtained from group-theoretical arguments outlined in Sec. II C. Similar effects were not observed at the spin-orbit split $E_0+\Delta_0$ transition in which no degeneracies are involved. Handler and co-workers[28] observed the effect of band warping on the polarization-dependent matrix element (7), again for the E_0 transition in Ge; by measuring surface-barrier spectra ($\vec{e}$ always $\perp \vec{F}$) they observed anisotropies characteristic of the unperturbed crystal only.

We have recently completed an extensive symmetry analysis of the E_1, E_0', and E_2 structures in Ge.[29] Portions of the E_0' spectrum were found to be independent of polarization for any direction of $\vec{F}$, which led to the first unambiguous determination of the crucial $\Gamma_{25'}-\Gamma_{15}$ separation. The spin-orbit splitting of the Γ_{15} conduction band was accurately obtained.

IV. LIMITATIONS

In closing, we point out some limitations of the analysis and indicate some areas that need further study.

In treating cubic materials, we have assumed that the effect of $\vec{F}$ is identical at diametrically opposite points $\vec{k}_i$ and $-\vec{k}_i$; this might require modification for more complex structures (the lack of inversion symmetry in III-V's has been neglected in similar studies[9,27]). It has recently been shown[30] that the electro-optic response in zinc-blende material consists of two contributions: electroreflectance, as described herein, which is even in $\vec{F}$, and piezoelectrically induced piezoreflectance, odd in $\vec{F}$. Only by experimentally separating the two can our symmetry analysis be applied.

The trial solution (3) assumes that the transition matrix elements are essentially constant over the spectral width of the transition. Although this cannot be rigorously justified, accounting for the effect of $\vec{F}$ on the matrix elements (discussed in Sec. II B) is the logical sequel to previous treatments.[8,9,12] Explicit calculation of matrix elements in the presence of $\vec{F}$ requires assumptions about the field-perturbed eigenfunctions; such calculations have not been performed to date.

In Sec. III, we considered the effect of an electric field perturbation on degenerate states in a cubic system, but omitted degeneracies resulting from equienergetic transitions at BZ points of different symmetries. The symmetry character of such a superposition will be more complex than considered so far, but still can be treated directly by using (4). For example, the polarization ratio signature (12) or (13) for two equienergetic transitions A and B having different symmetries would be

$$S=\frac{A_\perp+B_\perp}{A_\parallel+B_\parallel},$$

where both A and B would have the form $\sum f_i D_i$ of (4). The interpretation of such a signature is complicated by the fact that the response of the main peak and satellite structure will be affected differently as we rotate the sample with respect to $\vec{F}$ and $\vec{e}$, depending upon the superposition of the two structures. Such a superposition may occur at 3.4 eV in[15,27] Si and 4.4 eV in Ge.[17] In the case of transitions having twofold rotational symmetry or less, calculation of S becomes vastly more complicated. The orientation of $\vec{F}$ and $\vec{e}$ with respect to $\vec{k}_i$ must be specified by both polar and azimuthal angles, and the number of nonequivalent $\vec{k}_i$ becomes larger. As a practical matter, theoretical estimates of the principal components of the interband mass tensor would be required; these could then be tested experimentally.

ACKNOWLEDGMENTS

The authors acknowledge helpful conversations with V. Rehn, U. Rössler, R. Glosser, and B. Parsons, and many fruitful discussions with B. O. Seraphin.

*Research supported in part by the Humboldt Foundation.

[1]F. Herman, R. L. Kortum, C. D. Kuglin, and R. A. Short, in *Quantum Theory of Atoms, Molecules, and the Solid State*, edited by P. O. Löwdin (Academic, New York, 1966), p. 381; J. Phys. Soc. Japan Suppl. 21, 7 (1966).

[2]E. O. Kane, Phys. Rev. 146, 558 (1966).

[3]M. Cardona, F. H. Pollak, and K. L. Shaklee, J. Phys. Soc. Japan Suppl. 21, 89 (1966).

[4]F. Cerdeira, R. Lettenberger, and M. Cardona, Bull. Am. Phys. Soc. 12, 1049 (1967).

[5]B. O. Seraphin and N. Bottka, Phys. Rev. Letters 15, 104 (1965).

[6]V. Rehn and D. S. Kyser, Phys. Rev. Letters 18, 848 (1967).

[7]J. C. Phillips, Phys. Rev. 146, 584 (1966).

[8]N. Bottka and U. Rössler, Solid State Commun. 5, 939 (1967).

[9]F. Aymerich and F. Bassani, Nuovo Cimento B56, 295 (1968).

[10]D. D. Sell and E. O. Kane, Phys. Rev. 185, 1103 (1969); E. O. Kane, *ibid.* 178, 1368 (1969).

[11]R. Enderlein, R. Keiper, and W. Tausendfreund, Phys. Status Solidi 33, 69 (1969).

[12]D. E. Aspnes, Phys. Rev. 147, 554 (1966); 153, 972 (1967).

[13]D. E. Aspnes and N. Bottka, in *Semiconductors and Semimetals*, edited by R. K. Willardson and A. Beer (Academic, New York, to be published), Vol. VI.

[14]B. O. Seraphin and N. Bottka, Phys. Rev. 139, A560 (1965).

[15]B. O. Seraphin and N. Bottka, Phys. Rev. 145, 628 (1966).

[16]B. O. Seraphin, in *Semiconductors and Semimetals*, edited by R. K. Willardson and A. Beer (Academic, New York, to be published), Vol. VI.
[17]J. E. Fischer, N. Bottka, and B. O. Seraphin, Bull. Am. Phys. Soc. 14, 415 (1969).
[18]D. E. Aspnes and J. E. Rowe, Solid State Commun. 8, 1145 (1970).
[19]D. E. Aspnes, P. Handler, and D. Blossey, Phys. Rev. 166, 921 (1968).
[20]G. F. Koster, J. O. Dimmock, R. G. Wheeler, and H. Statz, *Properties of the Thirty-Two Point Groups* (MIT U. P., Cambridge, Mass., 1963).
[21]G. F. Koster, in *Solid State Physics*, edited by F. Seitz and D. Turnbull (Academic, New York, 1957), Vol. 5.
[22]S. C. Miller and W. F. Love, *Tables of Irreducible Representations of Space Groups and Co-Representations of Magnetic Space Groups* (Pruett, Boulder, Colo., 1967).
[23]G. F. Bassani, in *Proceedings of the International School of Physics "Enrico Fermi," Varenna*, 1965 (Academic, New York, 1966).
[24]J. E. Fischer and N. Bottka, Phys. Rev. Letters 24, 1292 (1970).
[25]A. K. Ghosh, Phys. Rev. 165, 888 (1968).
[26]J. E. Fischer, D. S. Kyser, and N. Bottka, Solid State Commun. 7, 1821 (1969).
[27]R. A. Forman, D. E. Aspnes, and M. Cardona, J. Phys. Chem. Solids 31, 227 (1970).
[28]P. Handler, S. Jasperson, and S. Koeppen, Phys. Rev. Letters 23, 1387 (1969).
[29]J. E. Fischer, in *Proceedings of the Tenth International Conference on the Physics of Semiconductors, Cambridge, Mass.*, 1970, edited by S. P. Keller, J. C. Hensel, and F. Stern (U. S. Atomic Energy Commission, Division of Technical Information, Washington, D. C., 1970).
[30]D. S. Kyser and Victor Rehn, Solid State Commun. 8, 1437 (1970).

PHYSICAL REVIEW B VOLUME 3, NUMBER 8 15 APRIL 1971

Electronic Conduction in Slightly Reduced Strontium Titanate at Low Temperatures*

C. Lee, J. Yahia, and J. L. Brebner
Département de Physique, Université de Montréal, Montréal, Québec, Canada

(Received 31 July 1970; revised manuscript received 2 November 1970)

The electronic transport properties of slightly reduced pure strontium titanate have been studied at low temperatures between 2 and 300 °K. The temperature dependence of resistivity, Hall coefficient, and Hall mobility showed different features from previous results for doped and reduced crystals with higher carrier concentrations. Specifically, the mobility at liquid-helium temperatures is small (5–700 cm^2/V sec) and increases with carrier concentration. Optical-absorption measurements showed the existence of several compensating acceptor levels and that the dominant mechanism of electron scattering was by longitudinal optical phonons at room temperature. Further, the data show that a specialized form of ionized-impurity scattering may play a role at low temperatures. A discussion of our experimental results is presented and it is concluded that an explanation of these in terms of a model of impurity-band conduction is appropriate.

I. INTRODUCTION

Electronic transport in semiconducting $SrTiO_3$ has been studied by several authors.[1–4] In the low-temperature studies, large electronic mobilities were found ranging from 10^3 to $2\times10^4\,cm^2/V\,sec$ for crystals with carrier concentrations between 10^{17} and $5\times10^{20}\,cm^{-3}$. According to Tufte and Chapman[2] and Frederikse *et al.*[3] the Hall mobility at liquid-helium temperature decreases with increasing carrier concentration and from this these authors concluded that the mobility at low temperatures was limited by ionized impurity scattering even though the magnitude of the theoretical and experimental values of mobility did not agree too well.

Tufte and Chapman[2] used the Mansfield formula[5] in the limit of large degeneracy to calculate mobility by ionized-impurity scattering at low temperatures and found that the calculated value was about 60 times larger than the experimental value for their Nb-doped sample. They attributed this large discrepancy to a compensation effect due to lattice defects. On the other hand, Frederikse *et al.*[3] followed Gulyaev's treatment[6] using the optical value for the dielectric constant in the expressions for the screening length and the effective Bohr radius. In this case theory underestimates the experimental mobility by a factor of 2–3 for the Nb- and La-doped samples, and overestimates by a factor of 2–4 for the hydrogen-reduced samples. Also, concentration dependence of mobility by theoretical calculation was much slower than that of experimental data. The validity of the use of the optical dielectric constant needs further discussion.

Another unexplained feature of the low-temperature results is that the mobility is much larger in the doped crystals than in the reduced samples.